Geoscience Letters

RESEARCH LETTER

Open Access

Intensity and timing of persistence barriers of global sea surface temperature anomalies

Feng Tian[1], Hong-Li Ren[1,2*], Minghong Liu[1], Baohuang Su[1] and Run Wang[1]

Abstract

Due to its intrinsic connection to predictability, persistence barrier (PB) has been known as a crucial property of some important phenomena like El Niño-Southern Oscillation (ENSO), typically depicted as a rapid decline of persistence of sea surface temperature (SST) anomalies occurring at a specific season. This study reveals the PB characteristics of the global SST anomalies by extending the ENSO PB diagnosis method to quantify the PB intensity and timing. A general PB intensity index is derived, and the PB timing is newly defined as the calendar month with the highest frequency of PB occurrence. Results show that the strong PBs of global SST anomalies are mainly distributed in the regions of the tropical Pacific and southeastern tropical Indian Ocean, corresponding to the well-known PB features. The PB timing varies globally and particularly shows an evolution along the equatorial Pacific band. These results could provide additional references for oceanic predictions.

Keywords Sea surface temperature, Persistence barrier, Persistence barrier intensity, Persistence barrier timing

Introduction

As one of the most important variables in the air–sea interface, sea surface temperature (SST) usually owns a better persistence than the atmosphere, and thus the SST anomaly has been widely used as a precursor in climate prediction (e.g., Goswami and Shukla 1991; Bengtsson et al. 1993; Trenberth et al. 1998; Peng et al. 2000; Frederiksen et al. 2001; Kang and Shukla 2006). However, in some areas, the persistence of SST anomalies shows a significant and rapid decline in specific seasons (Webster and Yang 1992). Such a phenomenon is called the persistence barrier (PB) and exists in many ocean regions around the world. It is well-known that there is a spring PB in the tropical Pacific related to El Niño-Southern Oscillation (ENSO), which usually emerges in the boreal spring and has an intrinsic connection to the ENSO predictability (Troup 1965; Wright 1979; Webster and Yang 1992; Xue et al. 1994; Torrence and Webster 1998; Clarke and van Gordon 1999, Yu and Kao 2007; Fang et al. 2019; Jin et al. 2021). With a diagnosis method, Ren et al. (2016) showed that the characteristics of PB are significantly different between the two types of ENSO, viz., the eastern Pacific (EP) and central Pacific (CP) types (e.g., Kao and Yu 2009; Kug et al. 2009; Ren and Jin 2011, 2013), where the EP ENSO PB occurs in late boreal spring with stronger PB, while the CP ENSO PB does in summer with weaker PB.

Besides the well-known ENSO PB, some studies have revealed PB phenomena of SST anomaly in other specific regions. In North Pacific, there is a PB during July–September (Namias and Born 1970; Ding and Li 2009), where particularly, a summer PB lies in the central-western North Pacific (CWNP) (Zhao et al. 2012) and the Kuroshio-Oyashio Extension (KOE) region (Duan and Wu 2015; Wu et al. 2016). In addition, PBs exist in the South China Sea (SCS) and Indonesia, where the SCS PB is in boreal autumn (October–November), while the

*Correspondence:
Hong-Li Ren
renhl@cma.gov.cn
[1] State Key Laboratory of Severe Weather, and Institute of Tibetan Plateau Meteorology, Chinese Academy of Meteorological Sciences, Beijing 100081, China
[2] Collaborative Innovation Center On Forecast and Evaluation of Meteorological Disasters (CIC-FEMD), Nanjing University of Information Science and Technology, Nanjing 210044, China

Indonesia PB is in early winter (November–December) (Chen et al. 2007; Zhao and Li 2009). A winter PB is in the southeastern tropical Indian Ocean (SEIO) (Nicholls 1984; Wajsowicz 2005), while the spring PB is in the western tropical Indian Ocean (WIO) (Luo et al. 2007). Indian Ocean dipole (IOD) also shows a significant winter PB (Ding and Li 2012; Feng and Duan 2014). It was shown that the spring PB of WIO is relatively weak, while the autumn SCS PB and the winter SEIO PB are stronger, and the winter PB exists in the northern tropical Atlantic (NTA) (Ding and Li 2011, 2012). A key question is what are and how to identify features of the PB timing and intensity in global SST?

In previous studies, the PBs, especially ENSO PB, have been determined qualitatively by the time with the worst persistence of SST anomaly indices (e.g., Webster and Yang 1992; McPhaden 2003; Yu and Kao 2007). To better understand the ENSO PB, Ren et al. (2016) proposed a quantitative method to measure the PB timing and intensity as the position and magnitude of the maximum lag-autocorrelation decline rate of the ENSO indices, which has been applied to predictability analysis and climate model evaluation (Ren et al. 2019; Tian et al. 2019). This study will examine the distinct characteristics of the PB timing and intensity in global SST anomalies by extending the ENSO PB diagnosis method of Ren et al. (2016) to a more general and appropriate sense.

Data and methods

Data

In this study, the monthly mean SST anomaly is obtained from the Hadley Centre Sea Ice and Sea Surface Temperature (HadISST) (Rayner et al. 2003) from 1981 to 2020 by eliminating the climatology and linear trend. The study has excluded grid points, where sea ice occurs.

Methods

The Niño3.4 index, defined as the SST anomaly average over (5°S–5°N, 170°–120°W), is used to introduce the quantitative method. Figure 1a shows a seasonally dependent persistence as represented by the lagged autocorrelation of the Niño3.4 index. With lag months

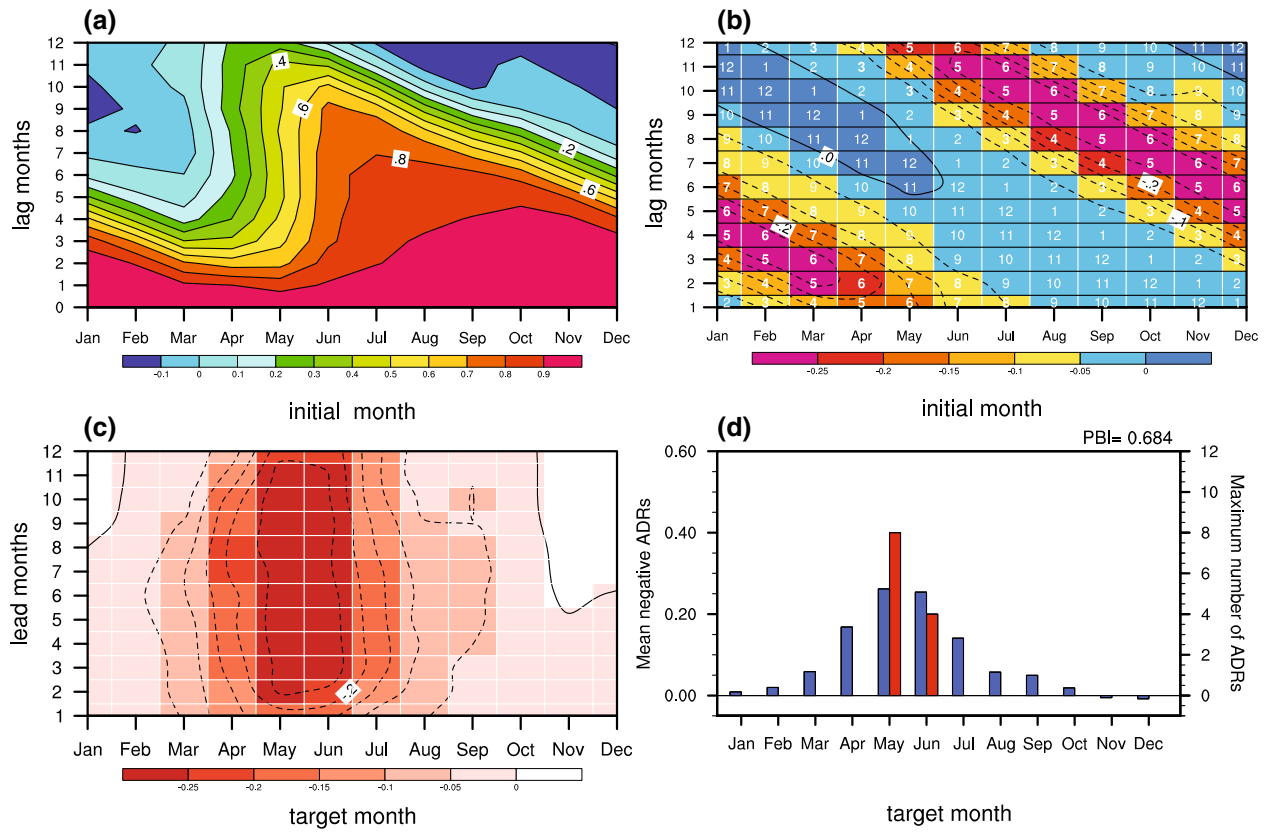

Fig. 1 **a** Autocorrelation as a function of initial calendar month (x axis) and lag month (y axis) for the Niño3.4 index. **b** Autocorrelation decline rates (ADRs) in (**a**). Values of the rate are plotted in contours and shaded boxes, respectively, where the interval is 0.05. White numbers in shaded boxes denote the target calendar month in the lag month domain. **c** ADRs as a function of target calendar month and lead month for the Niño3.4 index, where the interval is 0.05. **d** Mean ADRs for all 12 lead months (left y axis: blue bar) and the frequency of the maximum ADRs (right y axis: red bar) as a function of the target calendar month (x axis) for the Niño3.4 index

increasing, the autocorrelations first decline gradually, but abruptly at a specific month which is almost the same from different initial months. To quantify PB, Ren et al. (2016) proposed to directly utilize the maximum of the autocorrelation decline rate (ADR) as the measurement of PB in ENSO. Figure 1b shows the ADR of Niño3.4 index using the central difference:

$$G_j^i = \frac{C_{j+1}^i - C_{j-1}^i}{2} \quad (1)$$

where C denotes the autocorrelation,i the initial calendar month, j the lag month. In Fig. 1b, it can be clearly seen that the maximum decline rate basically occurs in May and June, indicating that in terms of the Niño3.4 index, the ENSO PB generally occurs in boreal late spring and early summer (from March to August).

To measure the broad features of PB of global SST anomalies, based on Fig. 1b, ADRs of the Niño3.4 index are further expressed as a function of the target calendar month and lead month (Fig. 1c), where the maximum ADRs overall emerge in May and June. In this way, the PB timing (PBT) can be defined as the target calendar month corresponding to the maximum of decline rates as averaged over all lead months (blue bars in Fig. 1d). On the other hand, by counting the frequency of the target calendar month with the maximum ADR from the 12 lead months, it is clearly found that May has the highest frequency of 8 occurrences, followed by June (4 occurrences) (red bars in Fig. 1d). Therefore, the PBT of Niño3.4 index from this viewpoint should be May as unique.

To measure the intensity that PB occurs, a general index representing PB intensity (PBI) can be further defined by revising the original PBI index proposed by Ren et al. (2016), viz., based on Fig. 1c, directly taking a negative summation of the ADRs of the 3 target months centered on the PBT. Then, taking the average over all of 12-lead months, the PBI of a certain SST index can be generally formulated as

$$PBI = -\frac{1}{12}\sum_{j=1}^{12}\sum_{k-1}^{k+1} G_k^j \quad (2)$$

where j denotes the lead month, k the target calendar month valuing the 3 months centered at the PBT, G_k^j the ADRs of the SST anomaly index for a given target calendar month and lead month. Still taking the Niño3.4 index as an example, the PBI is 0.684 (Fig. 1d).

To better represent the PBI of the 12 target months separately and its seasonal variation as well as corresponding relations with the PBT, Fig. 1d compares the mean negative ADRs of Niño3.4 index over 12-lead month domain (the average of y axis in Fig. 1c) with the number of maximum ADRs as a function of target month. It can be seen that the mean ADRs vary significantly with the target month and basically peak at the PBT that is defined as the calendar month with the highest frequency of PB occurrence. Negatively summing up the mean ADRs of during the 3 target months centered at the PBT just is the PBI of the index, equal to that from Eq. (2). The idealized autocorrelation coefficient decreases linearly at an average rate of 0.08 per month within 12-lag months. Here, it is noted that the PBT is meaningful when its PBI is greater than 0.3, referred to Fig. 1.

Results

The PBT and PBI of global SST anomalies are calculated by the above quantification methods and their distributions are shown in Fig. 2. The global distribution of PBT is characterized by a significant regional difference. The tropical Pacific and southeastern tropical Indian Ocean have strong PBs within a certain range, and there are also obvious PB phenomena in some parts of the global ocean.

In the tropical Pacific, the PBT of ENSO in the Niño3.4 region, particularly the EP ENSO PBT, is in May with a strong PB, while the CP ENSO PBT is in July with a weaker PB (Figs. 1d, 3a, b). This is consistent with the conclusion presented by Ren et al. (2016) that the EP ENSO PB occurs in late spring and the CP ENSO does in summer. Moreover, it is found that the PB of SST anomalies has an evolution feature along the longitude in the tropical Pacific, especially where ENSO emerges. The PBT evolves along the equatorial Pacific band from March in the east to August in the west with high PBI (Figs. 2, 3a, b), which might be related to the phase shift of the seasonal ocean–atmosphere feedback along the longitude (Ren et al. 2016; Liu et al. 2019).

In the low-latitude Northwestern Pacific (NWP; 5°–18°N, 135°–151°E), which is considered to be the area that ENSO can directly influence, there is an obvious PB and the PBT is in June and the PB is strong (Fig. 3c). The PB of the northern South China Sea (SCS) region (10°–20°N, 110°–120°E) as noted by Chen et al. (2007) is also verified. Our results show that its PBT is in October, which is consistent with the autumn PB found by them, and its PBI is relatively moderate, which is much smaller than the PBI in the southern SCS (Fig. 3d).

The Kuroshio-Oyashio Extension (KOE) SSTA plays a key role in regulating the weather and climate of the surrounding region. (Sun et al. 2008; Duan and Wu 2015). In this study, we have focused on the Kuroshio Source Region (KSR) (18°–24°N, 127°–138°E) and KOE region (38°–50°N, 153°E–177W°) to examine their PBs. It is clear that the KSR PBT is in January, while the KOE PBT is in June, with the PBI slightly stronger than the former (Fig. 3e, f). The central-western North Pacific (CWNP) (38°–46°N, 155°E–170°W), next to the KOE and studied

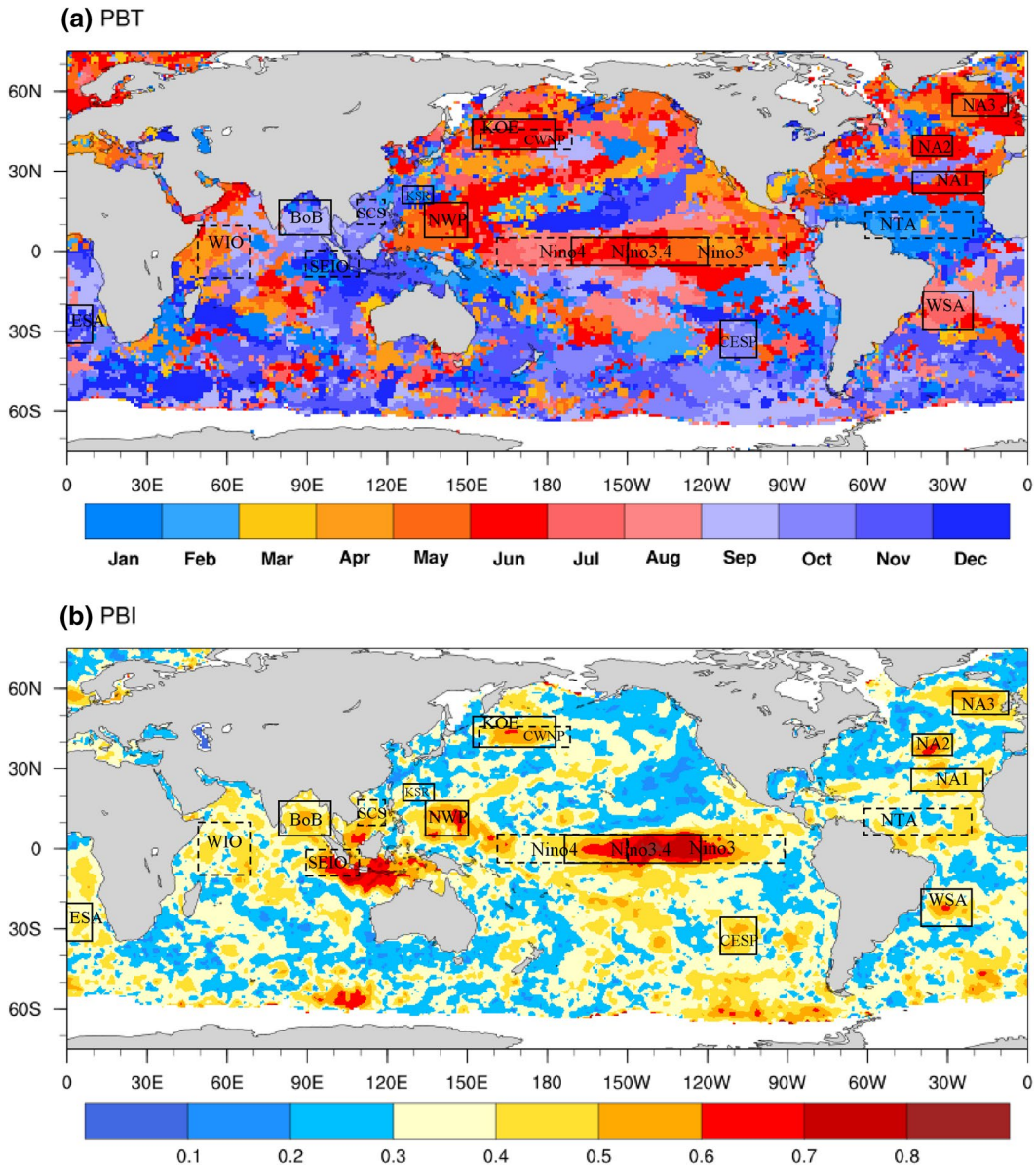

Fig. 2 **a** Global distribution of PBT. Shading is the PBT values. **b** Global distribution of PBI. Shading is the PBI values. The interference of sea ice has been removed. The dotted boxes are the area that others have studied. The solid boxes are the new specific area selected for this study

by Zhao et al. (2012), has shown that its PBT is also June, but the PBI is slightly weaker than that of the KOE (Fig. 3g). In the South Pacific, many studies have pointed out that the SSTA (0°–60°S,140°E–70°W) has obvious interannual variation, playing an important role in global climate change (Shaffer et al. 2000; Li et al. 2012). We selected the central-eastern South Pacific region (CESP; 25°–40°S, 100°–115°W), where PB is relatively strong with PBI of 0.489 and PBT is in October (Fig. 3h).

In the tropical Indian Ocean, there are evident boreal spring/summer PBs in the central and west parts, while a stronger autumn/winter PB in the east part, where the strongest PB is located in the southeast part (Fig. 2). To diagnose the PB feature of the Indian Ocean Dipole (IOD), the most well-known SST variability mode there (Saji et al. 1999), we focus on the western tropical Indian Ocean (WIO) (10°S–10°N, 50°–70°E) and the southeastern tropical Indian Ocean (SEIO) (10°S–0°, 90°–110°E). The diagnosis results show that the WIO PBT is in April as a boreal spring PB, and the SEIO PBT is in December as a winter PB with a much stronger PBI than the WIO PB (Fig. 4a, b). As a combination of these two parts, the

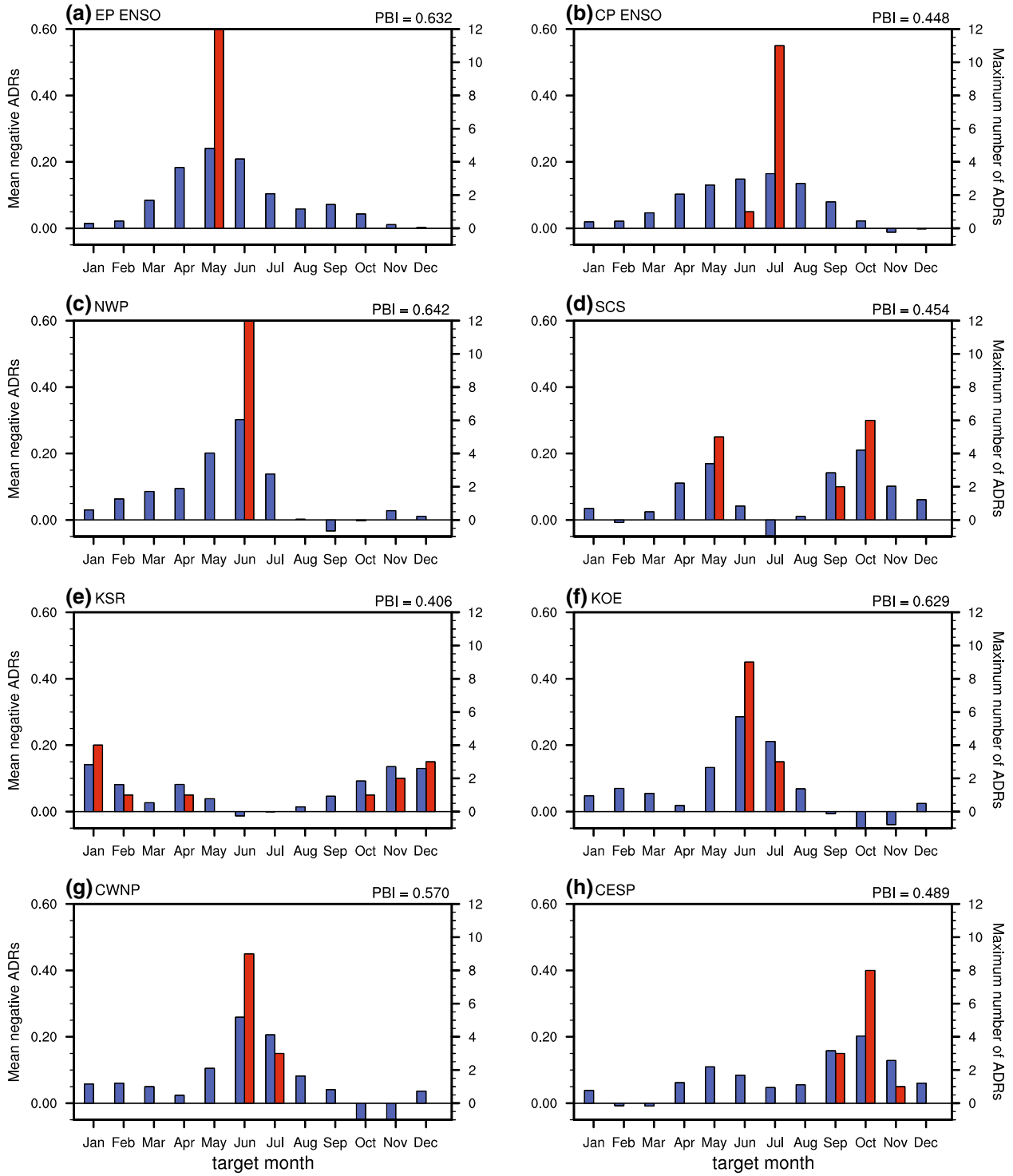

Fig. 3 Mean ADRs for all 12 lead months (left y axis) and the frequency of the maximum ADRs (right y axis) as a function of the target calendar month (x axis) for the **a** EP ENSO, **b** CP ENSO, **c** Northwestern Pacific (NWP), **d** northern South China Sea (SCS), **e** Kuroshio Source Region (KSR), **f** Kuroshio–Oyashio Extension region (KOE), **g** central-western North Pacific (CWNP), and **h** central-eastern South Pacific (CESP). Blue bar is the mean ADRs for all 12 lead months (left y axis), and red bar is the frequency of the maximum ADRs (right y axis)

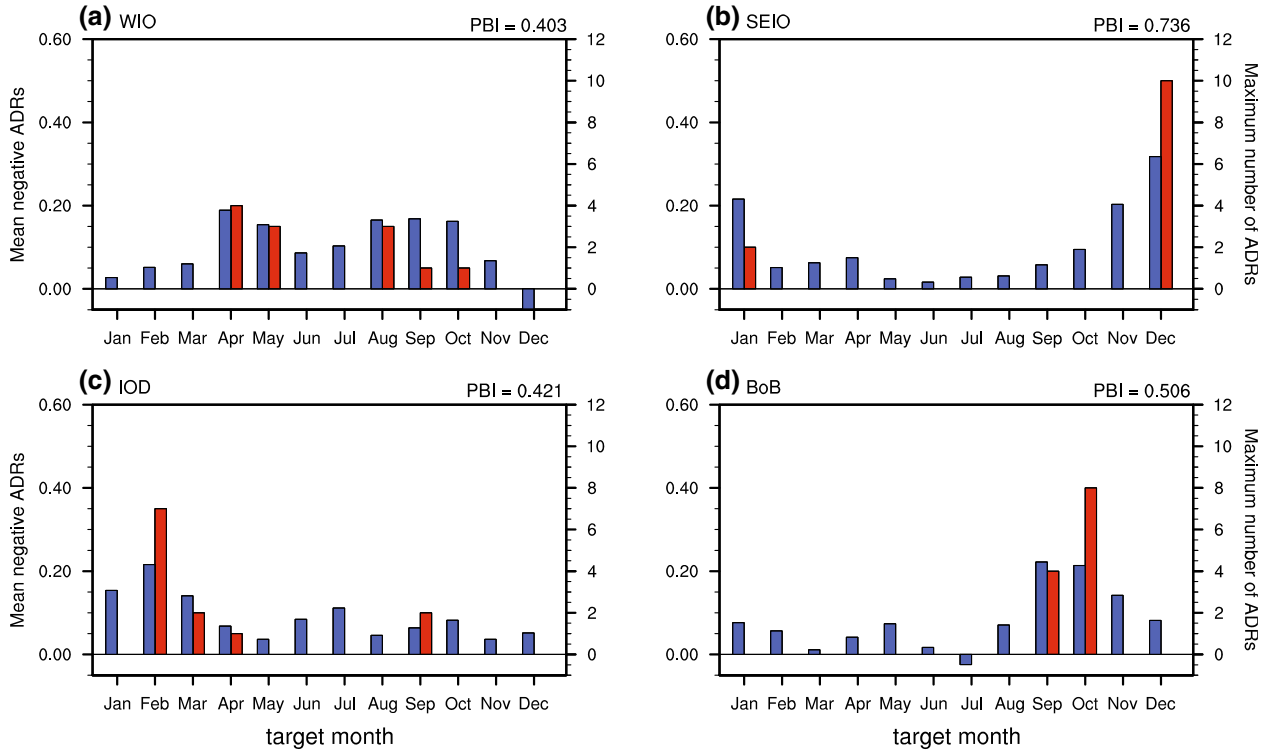

Fig. 4 Mean ADRs for all 12 lead months (left y axis) and the frequency of the maximum ADRs (right y axis) as a function of the target calendar month (x axis) for the **a** western tropical Indian Ocean (WIO), **b** southeastern tropical Indian Ocean (SEIO), **c** tropical Indian Ocean dipole (IOD), and **d** Bay of Bengal (BoB). Blue bar is the mean ADRs for all 12 lead months (left y axis), and red bar is the frequency of the maximum ADRs (right y axis)

IOD index is further verified for its PB properties, where PBT is in February with a moderate intensity (Fig. 4c). The results are basically consistent with those of previous studies (Ding and Li 2012; Liu et al. 2019). In the north Indian Ocean, the Bay of Bengal (BOB; 5°–20°N, 80°–110°E), a semi-enclosed sea in the northeastern Indian Ocean, has an important influence on the Indian monsoon (Goswami et al. 2022), which the PBI is also relatively large and the PBT is in October (Fig. 4d).

In the tropical Atlantic, obvious winter PBs exist in the central and west (Fig. 2), where SST anomalies in the northern tropical Atlantic (NTA) region (5°–15°N, 20°–60°W) noted by Ding and Li (2011) has a moderate PB with its PBT in January as a winter PB (Fig. 5a). In the North Atlantic, there are three regions with large PBI that may be associated with the North Atlantic SST tripole (NAST) pattern, the south lobe (22°–30°N, 16°–42°W), middle lobe (35–43°N, 27°–42°W), and north lobe (50°–60°N, 7°–27°W), respectively. All the three regions have PBT in June and the largest PBI in the middle (Fig. 5b–d). Meanwhile, we have examined the PB of the NAST index (Zuo et al. 2013), and the results show that its PB occurs in May with weak PBI (figure omitted). In the South Atlantic, interannual SST patterns may also contribute to the climate in South America, and the SSTA is considered to be one of the important factors in understanding the time scales variation of the South American Monsoon system (Marengo et al. 2012). Both the PBT and PBI are different between the east and west of the South Atlantic. The PBT of the eastern South Atlantic (ESA) (20°–35°S, 0°–10°E) is in December, while that of the western South Atlantic (WSA) (15°–30°S, 20°–39°W) is in July, with the stronger PB than WSA (Fig. 5e, f). In addition, PB also exists in a region of 50°–60°S, 100°–110°E in the Antarctic Sea, with a PBI of 0.630, and PBT in November.

Summary and discussion

This study focused on PB characteristics of the global SST anomalies by extending the ENSO PB diagnosis method that has been applied to predictability analysis and climate model evaluation (Ren et al. 2019; Tian et al. 2019) to quantify the PB intensity and timing. Here, the PBT has been newly defined as the calendar month with the highest frequency of PB occurrence, and a general PBI index has been defined to quantify the global SST anomalies PB by summing and averaging the ADRs of the 3 target months centered on the PBT in the 12-lead months domain. The global distribution of PBI clearly showed that strong PBs occur in the equatorial Pacific and southeastern tropical Indian Ocean, and there are

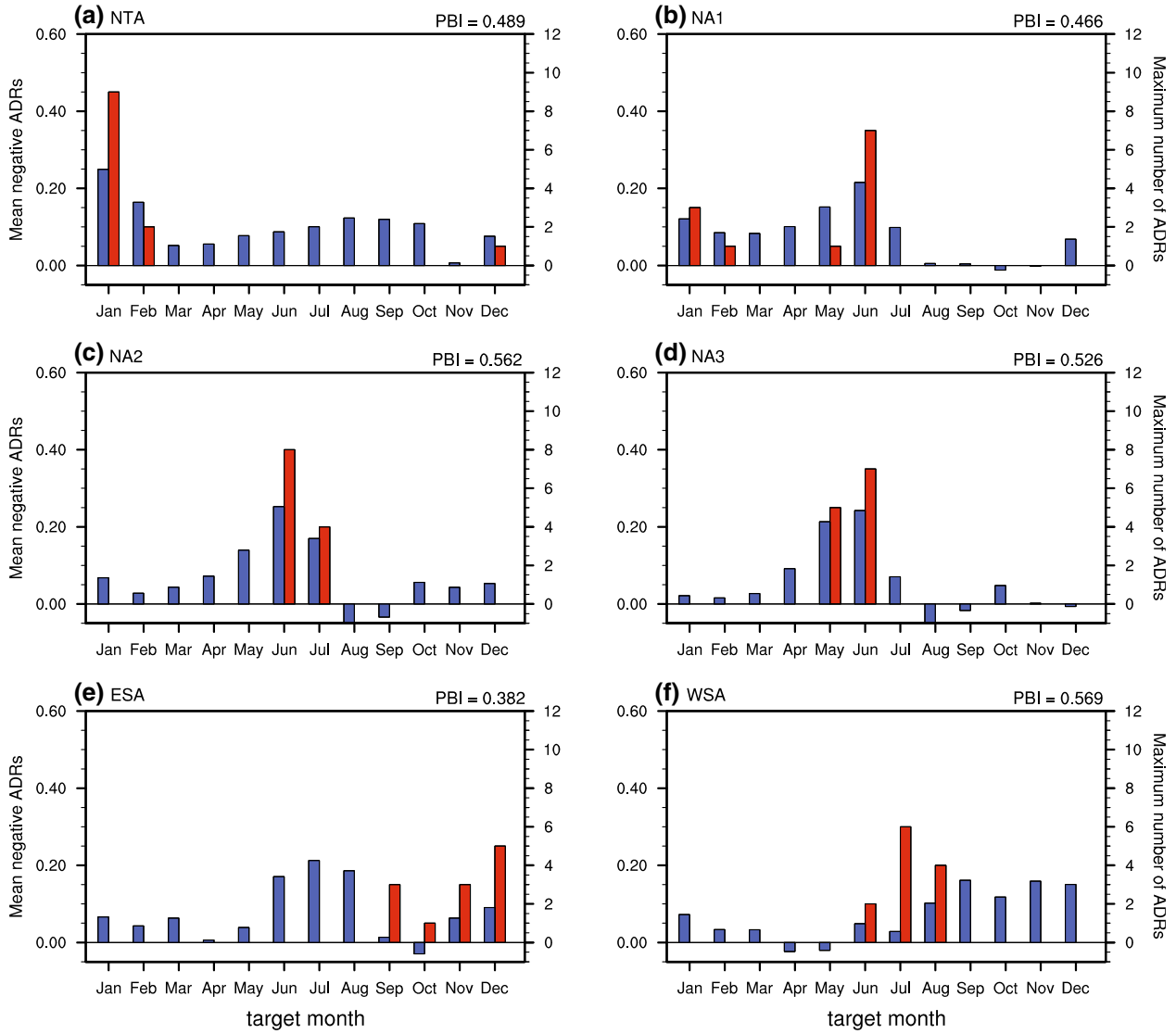

Fig. 5 Mean ADRs for all 12 lead months (left y axis) and the frequency of the maximum ADRs (right y axis) as a function of the target calendar month (x axis) for the **a** northern tropical Atlantic (NTA), **b** the south lobe of the three regions in the North Atlantic (NA1), **c** the middle lobe of the three regions in the North Atlantic (NA2), **d** the north lobe of the three regions in the North Atlantic (NA3), **e** eastern South Atlantic (ESA), and **f** western South Atlantic (WSA). Blue bar is the mean ADRs for all 12 lead months (left y axis), and red bar is the frequency of the maximum ADRs (right y axis)

also obvious PB phenomena in other parts of the global ocean, corresponding to both the well-known and newly discovered PB characteristics. Furthermore, the PB timing varies greatly by different regions and particularly shows an evolution feature in the equatorial Pacific region associated with ENSO.

Through the newly extended diagnosis methods, the PB timing and intensity could be determined more accurately and quantitatively. This would also provide an intuitionistic measure to interpret some spatiotemporal features and variations of ocean variables in model simulation and future projection from the perspective of persistence. Some studies have pointed out the potential influencing factors of PB characteristics in some regions (e.g., Chen et al. 2007; Zhao and Li 2009; Ding and Li 2011, 2012; Jin et al. 2019; Jin et al. 2021). However, from this paper, the PB intensity and timing are related but not the same and can be measured by different indices; whether they are both controlled by these factors needs more investigation. Moreover, why do the SST anomalies in the equatorial Pacific and SEIO show stronger PBs than other regions, and how

the evolution feature of PBs originates? These questions all need further efforts to address.

Author contributions

FT contributed to data analyses and wrote the manuscript; HLR supervised the study and provided the idea and revised the manuscript; MHL participated in part of the revision; BHS and RW gave some suggestions. All authors read and approved the final manuscript.

Funding

We thank two anonymous reviewers for their constructive suggestions. This work was jointly supported by the National Natural Science Foundation of China under Grants (42105067, 42105048, 42205047, 41975094), and the Basic Research and Operational Special Project of CAMS (2021Z007).

Availability of data and materials

HadISST data are obtained from the Met Office Hadley Centre, from the website at https://www.metoffice.gov.uk/hadobs/hadisst/

Declarations

Competing interests

The authors declare no competing financial interests.

Received: 8 October 2022 Accepted: 26 February 2023
Published online: 11 March 2023

References

Bengtsson L, Schlese U, Roeckner E, Latif M, Barnett TP, Graham NE (1993) A two-tiered approach to long-range climate forecasting. Science 261:1027–1029

Chen JM, Li T, Shih CF (2007) Fall persistence barrier of sea surface temperature in the South China Sea associated with ENSO. J Clim 20:158–172

Clarke AJ, van Gorder S (1999) The connection between the boreal spring Southern Oscillation PB and biennial variability. J Clim 12:610–620

Ding R, Li J (2009) Decadal and seasonal dependence of North Pacific sea surface temperature persistence. J Geophys Res. https://doi.org/10.1029/2008JD010723

Ding R, Li J (2011) Winter persistence barrier of sea surface temperature in the northern tropical Atlantic associated with ENSO. J Clim. https://doi.org/10.1175/2011JCLI3784.1

Ding R, Li J (2012) Influences of ENSO teleconnection on the persistence of sea surface temperature in the tropical Indian Ocean. J Clim 25(23):8177–8195

Duan WS, Wu YJ (2015) Season-dependent predictability and error growth dynamics of Pacific Decadal Oscillation-related sea surface temperature anomalies. Clim Dyn 44:1053–1072. https://doi.org/10.1007/s00382-014-2364-5

Fang X, Xie R (2019) A brief review of ENSO theories and prediction. Sci China. https://doi.org/10.1007/s11430-019-9539-0

Feng R, Duan W (2014) The spatial patterns of initial errors related to the "'winter predictability barrier"' of the indian ocean dipole. Atmos Ocean Sci Lett 7(5):406–410

Frederiksen CS, Zhang HQ, Balgovind RC, Nicholls N, Drosdowsky W, Chambers L (2001) Dynamical seasonal forecasts during the 1997/98 ENSO using persisted SST anomalies. J Clim 14:2675–2695

Goswami BN, Shukla J (1991) Predictability of a coupled ocean-atmosphere model. J Clim 4(1):3–22

Goswami BB, Murtugudde R, An SI (2022) Role of the Bay of Bengal warming in the Indian summer monsoon rainfall trend. Clim Dyn 59(5):1733–1751

Jin Y, Liu Z (2021) A theory of spring persistence barrier on ENSO. Part I: the role of ENSO period. J Clim. https://doi.org/10.1175/JCLI-D-20-0540.1

Jin Y, Liu Z, Lu Z, He C (2019) Seasonal period of background in the tropical Pacific as a cause of ENSO spring persistence barrier. Geophys Res Lett 46:13371–13378. https://doi.org/10.1029/2019GL085205

Jin Y, Liu Z, He C, Zhao Y (2021) On the formation mechanism of the seasonal persistence barrier. J Clim 34:479–494. https://doi.org/10.1175/JCLI-D-19-0502.1

Kang IS, Shukla J (2006) Dynamic seasonal prediction and predictability of the monsoon. In: Wang B (ed) The Asian Monsoon. Springer, Berlin, Heidelberg, pp 585–612

Kao HY, Yu JY (2009) Contrasting eastern-Pacific and central-Pacific types of El Niño. J Clim 22:615–632

Kug JS, Jin FF, An SI (2009) Two types of El Niño events: cold tongue El Niño and warm pool El Niño. J Clim 22:1499–1515

Li G, Li CY, Tan YK, Bai T (2012) Seasonal evolution of dominant modes in South Pacific SST and relationship with ENSO. Adv Atmos Sci 29(6):1238–1248. https://doi.org/10.1007/s00376-012-1191-z

Liu Z, Jin Y, Rong X (2019) A theory for the seasonal predictability barrier: threshold, timing, and intensity. J Clim 32:423–443

Luo JJ, Masson S, Behera S, Yamagata T (2007) Experimental forecasts of the Indian Ocean dipole using a coupled OAGCM. J Clim 20(10):2178–2190

Marengo JA, Liebmann B, Grimm AM, Misra V, Silva Dias PD, Cavalcanti IFA, Alves LM (2012) Recent developments on the South American monsoon system. Int J Climatol 32(1):1–21

McPhaden MJ (2003) Tropical Pacific Ocean heat content variations and ENSO persistence barriers. Geophys Res Lett 30(9):1480. https://doi.org/10.1029/2003GL016872

Namias J, Born RM (1970) Temporal coherence in North Pacific sea-surface temperature patterns. J Geophys Res 75:5952–5955

Nicholls N (1984) The Southern Oscillation and Indonesian sea surface temperature. Mon Wea Rev 112:424–432

Peng P, Kumar A, Barnston AG, Goddard L (2000) Simulation skills of the SST-forced global climate variability of the NCEP–MRF9 and the Scripps–MPI ECHAM3 models. J Clim 13:3657–3679

Rayner NA, Parker DE, Horton EB, Folland CK, Alexander LV, Rowell DP, Kent EC, Kaplan A (2003) Global analyses of sea surface temperature, sea ice, and night marine air temperature since the late nineteenth century. J Geophys Res 108(D14):4407. https://doi.org/10.1029/2002JD002670

Ren H-L, Jin F-F (2011) Niño indices for two types of ENSO. Geophys Res Lett 38:L04704. https://doi.org/10.1029/2010GL046031

Ren H-L, Jin F-F (2013) Recharge oscillator mechanisms in two types of ENSO. J Clim 26(17):6506–6523

Ren H-L, Jin F-F, Tian B, Scaife AA (2016) Distinct persistence barriers in two types of ENSO. Geophys Res Lett 43:10973–10979

Ren H-L, Zuo JQ, Deng Y (2019) Statistical predictability of Niño indices for two types of ENSO. Clim Dyn 52:5361–5382

Saji NH, Goswami BN, Vinayachandran PN, Yamagata T (1999) A dipole mode in the tropical Indian Ocean. Nature 401:360–363

Shaffer G, Leth O, Ulloa O, Bendtsen J, Daneri G, Dellarossa V, Hormazaball S, Sehlstedt PI (2000) Warming and circulation change in the eastern South Pacific Ocean. Geophys Res Lett 27(9):1247–1250

Sun JQ, Yuan W, Gao Y (2008) Arabian Peninsula-North Pacific Oscillation and its association with the Asian summer monsoon. Sci China Ser D Earth Sci 51:1001–1012

Tian B, Ren H-L, Jin F-F, Stuecker MF (2019) Diagnosing the representation and causes of the ENSO persistence barrier in CMIP5 simulations. Clim Dyn 53:2147–2160

Torrence C, Webster PJ (1998) The annual cycle of persistence in the El Nino/Southern Oscillation. Quart J Roy Meteorol Soc 124:1985–2004

Trenberth KE, Branstator GW, Karoly D, Kumar A, Lau N-C, Ropelewski C (1998) Progress during TOGA in understanding and modeling global teleconnections associated with tropical sea surface temperatures. J Geophys Res 103:14291–14324

Troup AJ (1965) The "southern oscillation." Quart J Roy Meteorol Soc 91:490–506

Wajsowicz RC (2005) Potential predictability of tropical Indian Ocean SST anomalies. Geophys Res Lett. https://doi.org/10.1029/2005GL024169

Webster PJ, Yang S (1992) Monsoon and ENSO—Selectively interactive systems. Quart J Roy Meteorol Soc 118(507):877–926

Wright PB (1979) Persistence of rainfall anomalies in the central Pacific. Nature 277:371–374

Wu Y, Duan W, Rong X (2016) Seasonal predictability of sea surface temperature anomalies over the Kuroshio-Oyashio Extension: low in summer and high in winter. J Geophys Res Oceans 121:6862–6873. https://doi.org/10.1002/2016JC011887
Xue Y, Cane MA, Zebiak SE, Blumenthal MB (1994) On the prediction of ENSO: a study with a low-order Markov model. Tellus 46:512–528
Yu J-Y, Kao H-Y (2007) Decadal changes of ENSO persistence barrier in SST and ocean heat content indices: 1958–2001. J Geophys Res Atmos 112:125–138
Zhao X, Li J (2009) Possible causes for the persistence barrier of SSTA in the South China Sea and the vicinity of Indonesia. Adv Atmos Sci 26:1125–1136. https://doi.org/10.1007/s00376-009-8165-9
Zhao X, Li JP, Zhang WJ (2012) Summer persistence barrier of sea surface temperature anomalies in the central western North Pacific. Adv Atmos Sci 29(6):1159–1173. https://doi.org/10.1007/s00376012-1253-2
Zuo JQ, Li WJ, Sun CH, Xu L, Ren H-L (2013) Impact of the North Atlantic sea surface temperature tripole on the East Asian summer monsoon. Adv Atmos Sci 30(4):1173–1186. https://doi.org/10.1007/s00376-012-2125-5

Publisher's Note